Circularly polarized luminescence of Eu(III) complexes with chiral 1,1'-bi-2-naphtol-derived bisphosphate ligands

Carlo Andrea Mattei, Kais Dhbaibi, Bertrand Lefeuvre, Vincent Dorcet, Gilles Argouarch, Olivier Cador, Boris Le Guennic, Olivier Maury, Claudia Lalli, Stéphan Guy, et al.

Circularly Polarized Luminescence of Eu(III) Complexes with Chiral BINOL-Derived Bisphosphate Ligands

Carlo Andrea Mattei,[1] Kais Dhbaibi,[1] Bertrand Lefeuvre,[1] Vincent Dorcet,[1] Gilles Argouarch,[1] Olivier Cador,[1] Boris Le Guennic,[1] Olivier Maury,[2] Claudia Lalli,[1] Stéphan Guy,[3] Amina Bensalah-Ledoux,[3] François Riobé,*[2] Bruno Baguenard,*[3] Fabrice Pointillart*[1]

[1] *Univ Rennes, CNRS, ISCR (Institut des Sciences Chimiques de Rennes) – UMR 6226, 35000 Rennes (France)*

E-mail: fabrice.pointillart@univ-rennes1.fr

[2] *Univ Lyon, ENS de Lyon, CNRS UMR 5182, Laboratoire de Chimie, 69342, Lyon (France)*

E-mail: francois.riobe@ens-lyon.fr

[3] *Univ Lyon, Université Claude Bernard Lyon 1, CNRS, UMR 5306, Institut Lumière Matière, 69622 Lyon (France)*

E-mail: bruno.baguenard@univ-lyon1.fr

Abstract

The interest for lanthanide circularly polarized luminescence (CPL) has been quickly growing for ten years. However, very few of these studies have involved correlation between the dissymmetry factor (g_{lum}) and the chemical modifications in a series of chiral ligands. Four polymeric compounds of Eu(III) were prepared by using a series of binaphtyl derivatives for which the size of the π system as well as the number of stereogenic elements (i.e. the binaphtyl moiety) are modulated. The resulting $\{[Eu(hfac)_3((S)/(R)\text{-}L^x)]\}_n$ (x = 1 and 3) and $\{[Eu(hfac)_3((S,S,S)/(R,R,R)\text{-}L^x)]\}_n$ (x = 2 and 4) have been characterized by powder X-ray diffraction by comparison with the X-ray structures on single crystal of the Dy(III) analogues. In solution, the structure of the complexes is deeply modified and become monomeric. The nature of the ligand induces change in the shape of the CPL spectra in CH_2Cl_2 solution. Furthermore a large $|g_{lum}|$ = 0.12 of the magnetic-dipole transition for the $[Eu(hfac)_3((S,S,S)/(R,R,R)\text{-}L^2)]$ complex involving the ligand with three stereogenic elements and an extended π system has been measured. This report also shows CPL measurements in

solid-state for the series of $\{[Eu(hfac)_3((S)/(R)\text{-}L^x)]\}_n$ (x = 1 and 3) and $\{[Eu(hfac)_3((S,S,S)/(R,R,R)\text{-}L^x)]\}_n$ (x = 2 and 4) polymers.

Keywords: Binol, Bisphosphate, Europium, Circular Dichroism, Circularly Polarized Luminescence

1. INTRODUCTION

The difference of intensity between the emissions of left- and right-circularly polarized light by chiral molecular materials defines the Circularly Polarized Luminescence (CPL).[1,2] The growing interest for this kind of materials comes from their potential applications in 3D-displays,[3] data storage[4] and biomolecular processes[5,6]. The dissymmetry factor (g_{lum}) is a convenient way to express the CPL activity with $g_{lum} = 2(I_L - I_R)/(I_L+I_R)$, where I_L and I_R stand for the intensity of the left- and right-circularly polarized emissions, respectively. As a result from the previous expression, the g_{lum} factor ranges from -2 to +2 values. A wide variety of chiral organic molecules has been developed to observed CPL, for instance organic dyes,[7-12] helicenes,[9,13-17] cyclohexane diamine[18] and pyridinebisoxazoline[19]. Nevertheless, the g_{lum} values for such chiral organic molecules are often in the 10^{-4} to 10^{-2} range.[20-22] Since the 4*f*-4*f* transitions are Laporte forbidden in the lanthanide compounds, both static and dynamic coupling mechanisms[23,24] are at the origin of the electric dipole transition strength. The magnetic dipole transitions are allowed (as long as $\Delta J = 0, \pm 1$) and can dominate leading to larger rotatory strengths compared with the electric dipole ones, resulting in larger g_{lum}. The most known magnetic dipole transition which leads to large emission g_{lum} value is the $^5D_0 \rightarrow {}^7F_1$ transition within the $4f^6$ configuration of Eu(III). Thus, the highest value of g_{lum}=1.38 was measured for the Cs[Eu((+)-hfbc)$_4$] complex (where hfbc=3-heptafluorobutylryl-(+)-camphorato)[25] and has motivated numerous CPL studies involving chiral europium complexes.[6,26-34] The Laporte forbidden 4*f*-4*f* transitions have very weak absorption coefficient and their direct excitation can be inefficient. Then, the chiral ligand should act as an efficient organic chromophore for the lanthanide sensitization.[35,36] Among the plethora of chiral organic chromophores able to both sensitize the lanthanide luminescence and to allow chiroptical properties,[37,38] ligands with axial chirality such as the binaphtyl derivatives are good candidates. Indeed, their enantioselective preparations are easily accessible and several studies in the literature demonstrated that $\pi \rightarrow \pi^*$ transitions can sensitize lanthanide luminescence and the resulting coordination compounds gave observable CPL.[39-45] However, very few studies have

involved correlation between the dissymmetry factor (g_{lum}) and the chemical modifications within a series of chiral ligands based on a common molecular platform.[46,47]

In the following lines, four chiral 1,1'-Bi-2-naphtol (BINOL)-derived bisphosphate ligands (((*S*)/(*R*))-L^x (x = 1 and 3) and ((*S,S,S*)/(*R,R,R*))-L^x (x = 2 and 4) ligands[48]) were selected to elaborate Eu(III)-based compounds (Scheme 1). Among this series of four ligands, the size of the π-system as well as the number of stereogenic elements were modulated. The influence of the chiral ligand on the metal-centered CPL was investigated both in solution and solid-state.

2. MATERIALS AND METHODS

The precursors $Eu(hfac)_3(H_2O)_2$ ($hfac^-$ = 1,1,1,5,5,5-hexafluoroacetylacetonate anion),[49] ((*S*)/(*R*))-L^x (x = 1 and 3) and ((*S,S,S*)/(*R,R,R*))-L^x (x = 2 and 4) ligands[48] were synthesized following previously reported methods. All other reagents were purchased from Merck Co., Inc. and used without further purification. All solid-state characterization studies (elementary analysis, IR, PXRD, magnetic susceptibility and photophysical measurements) were performed on dried samples and are considered without solvent of crystallization.

The elemental analyses of the compounds were performed at the Centre Régional de Mesures Physiques de l'Ouest, Rennes.

^1H, ^{31}P NMR and ^{19}F NMR spectra were recorded using Bruker Avance spectrometers at 400 MHz for ^1H NMR, 376 MHz for ^{19}F NMR and 162 MHz for ^{31}P NMR. Chemical shifts (δ) are reported in parts per million (ppm) relative to TMS. The coupling constants (J) are given in hertz (Hz) and the corresponding multiplicity (s = singlet, d = doublet, t = triplet, m = multiplet).

2.1 Preparation of the complexes $\{[Ln(hfac)_3((S)/(R)\text{-}L^x)]\}_n$ (Ln = Eu and Dy) (x = 1-4)

$\{[Eu(hfac)_3((S)/(R)\text{-}L^1)]\}_n$ ($[(S)/(R)\text{-}1]_n$).

32.4 mg (0.04 mmol) of $[Eu(hfac)_3(H_2O)_2]$ were added to a solution containing 30.0 mg (0.04 mmol) of (*S*)-L^1 or (*R*)-L^1 in 2 mL of CH_2Cl_2. After 15 minutes of stirring, 80 mL of n-hexane were layered. After several days, the solution was slowly evaporated leading to a colourless and microcrystalline solid. 42.3 mg, 69 % yield for **$[(S)\text{-}1]_n$** and 51.5 mg, 84 % yield for **$[(R)\text{-}1]_n$**. Anal. Calcd (%) for $C_{59}H_{35}EuF_{18}O_{14}P_2$ (**$[(S)\text{-}1]_n$**): C 46.46, H 2.30; found: C 46.09, H 2.40. Anal. Calcd (%) for $C_{59}H_{35}EuF_{18}O_{14}P_2$ (**$[(R)\text{-}1]_n$**): C 46.46, H 2.30; found: C 46.14, H 2.36. Slow evaporation from a solution in CH_2Cl_2/*n*-hexane led to single crystals of **$[(R)\text{-}1]_n$** suitable for X-ray diffraction studies. Representative I.R. (KBr; range 1800–400 cm^{-1}): 1654 (s), 1591

(m), 1558 (m), 1526 (m), 1489 (s), 1456 (w), 1254 (s), 1194 (s), 1144 (s), 1101 (m), 1079 (m), 1029 (s), 1015 (s), 1005 (m), 994 (m), 968 (m), 951 (m), 902 (w), 875 (w), 869 (w), 850 (w), 821 (m), 807 (m), 796 (m), 779 (m), 763 (m), 753 (m), 740 (w), 704 (w), 686 (m), 662 (m), 615 (w), 585 (m), 558 (w), 554 (w), 526(w), 517 (w), 502(w), 495 (w), 482 (w), 464 (w) and 457 (w) cm^{-1}. $[\alpha]_D^{25} = +45$ for **[(*S*)-1]** and $[\alpha]_D^{25} = -43$ for **[(*R*)-1]** (c = 1.0, $CHCl_3$).

{[Eu(hfac)$_3$((*S,S,S*)/(*R,R,R*))-L^2)]}$_n$ ([(*S,S,S*)/(*R,R,R*)-2]$_n$).

A solution of 48.5 mg (0.06 mmol) of [Eu(hfac)$_3$(H_2O)$_2$] in 5 mL of CH_2Cl_2 was added to a solution of 56.8 mg (0.06 mmol) of (*S,S,S*)-L^2 or (*R,R,R*)-L^2 in 5 mL of CH_2Cl_2. After 15 minutes of stirring, 30 mL of *n*-hexane were layered. Slow diffusion led to colourless single crystals which were suitable for X-ray studies. 90.8 mg, 88 % yield in crystals for **[(*S,S,S*)-2]$_n$** and 87.6 mg, 84 % yield in crystals for **[(*R,R,R*)-2]$_n$**. Anal. calcd (%) for $C_{75}H_{39}EuF_{18}O_{14}P_2$ **[(*S,S,S*)-2]$_n$**: C 52.36, H 2.27; found: C 52.31, H 2.31. I.R. Anal. calcd (%) for $C_{75}H_{39}EuF_{18}O_{14}P_2$ **[(*R,R,R*)-2]$_n$**: C 52.36, H 2.27; found: C 52.29, H 2.33. Representative I.R (KBr, range 1800–400 cm^{-1}): 1654 (s), 1591 (w), 1555 (m), 1527 (m), 1491 (s), 1256 (s), 1201 (s), 1147 (s), 1102 (m), 1074 (m), 1027 (m), 1018 (m), 992 (m), 971 (w), 962 (w), 808 (w), 798 (m), 778 (w), 754 (m), 741 (w), 687 (w), 661 (m), 586 (m), 527 (w), 507 (w) and 466 (w) cm^{-1}. $[\alpha]_D^{25} = +131$ for **[(*S,S,S*)-2]** and $[\alpha]_D^{25} = -141$ for **[(*R,R,R*)-2]** (c = 1.0, $CHCl_3$). ^{1}H NMR (400 MHz, CD_2Cl_2) δ 11.52 (s, 2H), 8.96 (s, 2H), 8.59 (s, 2H), 8.38 (s, 2H), 8.07 (d, J = 8.6 Hz, 4H), 7.86 (d, J = 7.2 Hz, 4H), 7.58 (t, J = 7.6 Hz, 2H), 7.45 (d, J = 8.2 Hz, 2H), 7.33 (t, J = 7.7 Hz, 2H), 7.28 – 7.16 (m, 6H), 7.04 (t, J = 7.7 Hz, 2H), 6.95 (d, J = 10.4 Hz, 4H), 6.52 (s, 4H), 6.05 – 5.93 (m, 2H), 2.44 (d, J = 50.7 Hz, 3H) (Figure S1). ^{31}P NMR (162 MHz, CD_2Cl_2) δ -105.41 (Figure S2). ^{19}F NMR (376 MHz, CD_2Cl_2) δ -80.45 (Figure S3).

{[Eu(hfac)$_3$((*S*)/(*R*))-L^3)]$_3$}$_n$ ([(*S*)/(*R*)-3]$_n$).

32.4 mg (0.04 mmol) of [Eu(hfac)$_3$(H_2O)$_2$] were added to a solution of 30.3 mg (0.04 mmol) of (*S*)-L^3 or (*R*)-L^3 in 2 mL of CH_2Cl_2. After 15 minutes of stirring, 80 mL of *n*-hexane were layered. After several days, the solution was slowly evaporated leading to a colourless and microcrystalline solid. 42.4 mg, 69 % yield for **[(*S*)-3]$_n$** and 45.3 mg, 74 % yield for **[(*R*)-3]$_n$**. $C_{177}H_{129}Eu_3F_{54}O_{42}P_6$ **[(*S*)-3]$_n$**: C 46.24, H 2.81; found: C 46.09, H 2.90. $C_{177}H_{129}Eu_3F_{54}O_{42}P_6$ **[(*R*)-3]$_n$**: C 46.24, H 2.81; found: C 46.12, H 2.87. Representative I.R. (KBr, range 3200–400 cm^{-1}): 3077 (w), 2937 (w), 2863 (w), 1653 (s), 1591 (w), 1555 (m), 1527 (m), 1491 (s), 1256 (s), 1201 (s), 1147 (s), 1102 (m), 1075 (m), 1027 (m), 1018 (m), 992 (m), 971 (w), 962 (w), 808 (w), 798 (m), 778 (w), 755 (m), 741 (w), 687 (w), 661 (m), 586 (m), 529 (w), 507 (w) and

466 (w) cm^{-1}. $[\alpha]_D^{25} = -9.2$ for **[(*S*)-3]** and $[\alpha]_D^{25} = +9.4$ for **[(*R*)-3]** (c = 1.0, $CHCl_3$). ^{1}H NMR (400 MHz, CD_2Cl_2) δ 11.52 (s, 4H), 8.74 (s, 4H), 8.43 – 7.99 (m, 4H), 7.05 – 6.56 (m, 12H), 3.40 (s, 3H), 2.93 (d, *J* = 17.3 Hz, 2H), 2.72 (dq, *J* = 12.9, 6.5 Hz, 4H), 2.32 (d, *J* = 17.0 Hz, 2H), 1.93 – 1.61 (m, 6 H), 1.50 (s, 2H) (Figure S4). ^{31}P NMR (162 MHz, CD_2Cl_2) δ -147.12 (Figure S5). ^{19}F NMR (376 MHz, CD_2Cl_2) δ -79.95 (Figure S6).

{[Eu(hfac)$_3$((*S,S,S*)/(*R,R,R*))-L^4)]}$_n$ ([(*S,S,S*)/(*R,R,R*)-4]$_n$).

A solution of 5 mL of toluene containing 58.3 mg (0.06 mmol) of (*S,S,S*)-L^4 or (*R,R,R*)-L^4 was added to a suspension of 48.5 mg (0.06 mmol) of [Eu(hfac)$_3$(H_2O)$_2$] in 3 mL of toluene. The resulting solution was stirred for 15 minutes. Slow diffusion of n-pentane led to colourless crystals suitable for X-ray studies. 67.9 mg, 65 % yield in crystals for **[(*S,S,S*)-4]$_n$** and 73.1 mg, 70 % yield in crystals for **[(*R,R,R*)-4]$_n$**. Anal. calcd (%) for $C_{75}H_{63}EuF_{18}O_{14}P_2$ (**[(*S,S,S*)-4]$_n$**): C 51.64, H 3.61; found: C 51.75, H 3.66. Anal. calcd (%) for $C_{75}H_{63}EuF_{18}O_{14}P_2$ (**[(*R,R,R*)-4]$_n$**): C 51.64, H 3.61; found: C 51.71, H 3.55. Representative I.R. (KBr, range 3200–400 cm^{-1}): 2938 (m), 2863 (w), 1655 (s), 1556 (m), 1527 (m), 1501 (m), 1469 (m), 1255 (s), 1208 (s), 1148 (s), 1102 (m), 1073 (w), 1056 (m), 1015 (m), 993 (m), 969 (m), 909 (w), 890 (w), 832 (w), 797 (w), 663 (m), 587 (w) and 528 (w) cm^{-1}. $[\alpha]_D^{25} = +13$ for **[(*S,S,S*)-4]** and $[\alpha]_D^{25} = -13$ for **[(*R,R,R*)-4]** (c = 1.0, $CHCl_3$). ^{1}H NMR (400 MHz, CD_2Cl_2) δ 9.20 (s), 8.27 (s,), 7.88 – 6.48 (m), 3.61 – 2.54 (m), 2.51 – 2.26 (m), 2.25 – 1.46 (m) (Figure S7). ^{19}F NMR (376 MHz, CD_2Cl_2) δ -79.97 (Figure S8).

2.2 X-ray Structure Analysis

Single crystal were mounted on a D8 VENTURE Bruker-AXS diffractometer for cell determination for **[(*S*)/(*R*)-3]$_n$** (Table S1) and data collection for {[Dy(hfac)$_3$((*S*)-L^3)]$_3$}$_n$ (Table S2) (MoKα radiation source, λ = 0.71073 Å) from the Centre de Diffractométrie X (CDIFX), Université de Rennes 1, France. Structures were solved with direct methods using the SHELXT Program[50] and refined with a full matrix least-squares method on F2 using the SHELXL-14/7 program.[51] Crystallographic data for the structure reported in this paper have been deposited with the Cambridge Crystallographic Data Centre (insert CCDC 2093298). Copies of the data can be obtained, free of charge, on application to the Director, CCDC, 12 Union Road, Cambridge CB2 1EZ, United Kingdom (Fax: 44-1223-336033 or e-mail: deposite@ccdc.cam.ac.uk. X-ray diffraction (XRD) patterns for all samples were recorded at room temperature in the 2θ range 5–30° with a step size of 0.026° and a scan time per step of 600 s using a PANalytical X'Pert Pro diffractometer (Cu-L2,L3 radiation, λ = 1.5418 Å, 40 kV,

40 mA, PIXcel 1D detector). Data collector and HighScore Plus software were used, respectively, for recording and analyzing the patterns.

2.3 Spectroscopic Analysis

Optical rotations were recorded with a Perkin Elmer Model 341 polarimeter. Absorption spectra were recorded on a JASCO V-650 spectrophotometer in diluted solution by using spectrophotometric grade solvents. Electronic circular dichroism (ECD) was measured on a Jasco J-815 Circular Dichroism Spectrometer (IFR140 facility – Biosit-Université de Rennes 1). Emission spectra were measured using Horiba-Jobin–Yvon Fluorolog-3 fluorimeter. The steady-state luminescence was excited by unpolarized light from a 450 W xenon continuous wave (CW) lamp and detected at an angle of 90° for dilute solutions (10 mm quartz cuvette) or solid (4 mm quartz tube) by using a Hamamatsu R928 PMT detector. Scattered excitation light was filtered thanks to appropriate long-pass filters. Luminescence decay plots were obtained by pulsed excitation using a FL-1040 UP Xenon Lamp and lifetimes were obtained by an exponential least-squares fitting using Origin®.

A homemade CPL apparatus based on a standard photo-elastic modulator (PEM 100 from Hinds company) – polarizer arrangement[1] was used. The samples are excited with low cost unpolarized UV LED. The emitted light is collected with a lens and directs to the PEM and the following Glan polarizer (neutral axes at 45 degrees of that one of the PEM). A second lens focus the light on the entrance slit of a monochromator (Cornerstone 260 from Newport). A photomultiplier tube (PM Hamamatsu R1477-06) is used as detector and the electric signal is measured by a Keythley multimeter for the DC signal UDC and a Standford SR830 LockIn Amplifier for the 1f modulated signal U1F. The fluorescence signal is given by the DC part of the signal while the CPL is the U1F corrected by factor of sqrt(2) and the first kind Bessel function J1(2.405), where 2.405 is the retardance amplitude of the PEM.[1] Two excitation schemes are used for liquid or powder samples. UV LED is fixed on the “back” side of the cuvette. This allows a longitudinal excitation scheme without any polarization selection and an easy alignment. For solid state samples, the carefully ground powder is deposited on the sample holder (a glass covered sample) placed at around 45 degrees of the collection angle and the UV light is placed at the opposite.

3. RESULTS AND DISCUSSION

3.1 Structural Analysis

The X-ray structure of **[(*R*)-1]**$_n$[52] and the dysprosium analogues of **[(*S*,*S*,*S*)-2]**$_n$ and **[(*S*,*S*,*S*)-4]**$_n$[53] were previously determined on single crystal and their purity phase was checked for both enantiomers by powder X-ray diffraction. The quality of the single crystals of **[(*S*,*S*,*S*)-2]**$_n$, **[(*S*)-3]**$_n$ and **[(*S*,*S*,*S*)-4]**$_n$ did not allow a satisfying refinement of the structures. Their isostructural and purity phases were checked by powder X-ray diffraction (Figures S9-S11). For **[(*S*,*S*,*S*)-4]**$_n$, fast loss of crystallographic solvent molecules led to a loss of crystallinity of the powder (Figure S11) and a determination of the cell parameters was done (Table S1). Finally suitable single crystals of the dysprosium analogue of **[(*S*)-3]**$_n$ were obtained and its X-ray structure is described in Supporting Information (Figures S12 and S13). The isostructural and purity phases of **[(*S*)-3]**$_n$ were checked by powder X-ray diffraction (Figure S14).

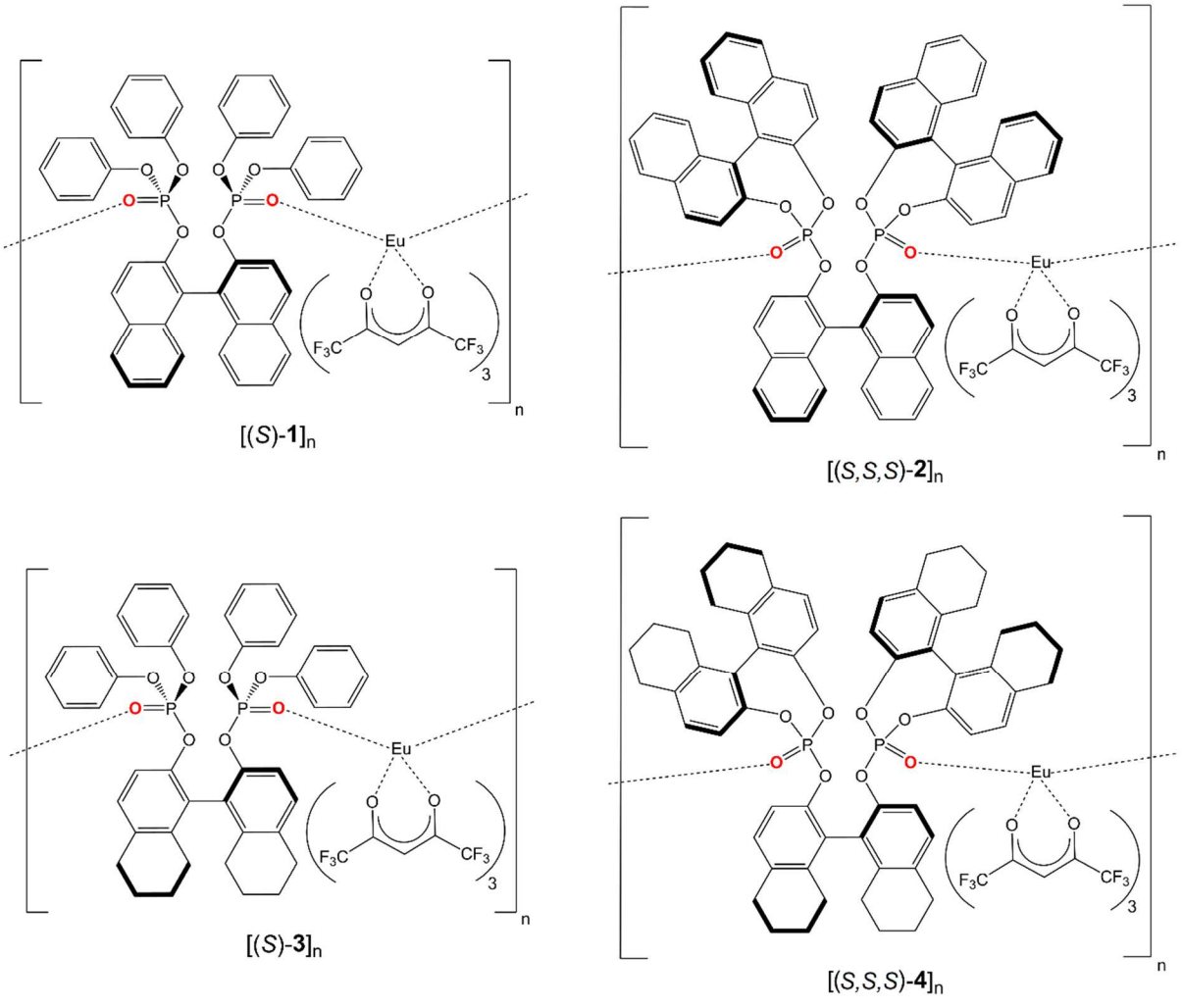

Scheme 1. Molecular structures of the (*S*)-enantiomer of the four polymers obtained in the solid state **[(*S*)-1]**$_n$, **[(*S*,*S*,*S*)-2]**$_n$, **[(*S*)-3]**$_n$ and **[(*S*,*S*,*S*)-4]**$_n$.

3.2 Optical Analysis

3.2.1 UV-visible Absorption and CD measurements

The UV-visible absorption and ECD spectra for the complexes **[(*S/R*)-1]**, **[(*S,S,S/R,R,R*)-2]**, **[(*S/R*)-3]** and **[(*S,S,S/R,R,R*)-4]** in CH_2Cl_2 solution are presented in Figures S15-S18. It was previously demonstrated by NMR studies and DFT calculations that the coordination polymer $\{[Eu(hfac)_3(S/R\text{-}L^1)]\}_n$ is fragmented to monomeric species by its solubilization.[52] The suggested structure of the monomeric specie is depicted in Figure S19. The fragmentation of the polymeric structure is accompanied with a reorganisation of both $hfac^-$ anions and binaphtyl-based ligand. The latter acts as a bidentate ligand (Figure S19). Thus, n = 1 for the complexes in solution. The experimental absorption curves for the two enantiomers of each complexes are composed of broad bands localized at the intermediate energy range of 30–40 000 cm^{-1} and at high energy (above 43–45 000 cm^{-1}) which are mainly attributed to the π–π* transitions of the binaphthyl-like moieties with a contribution of the π–π* transitions of the $hfac^-$ anions known to be localized at 33000 cm^{-1}.[54] It is worth to notice that the maxima of the highest-energy absorption bands are not observed in the experimental 25000-45000 cm^{-1} range for the complexes involving the partially hydrogenated ligands (**[(*S/R*)-3]** and **[(*S,S,S/R,R,R*)-4]**) (Figures S17a and S18a).

ECD spectra confirm the enantiomeric nature of the complexes in CH_2Cl_2 solution at room temperature. A correspondence between the ECD and absorption bands can be observed. The ECD signals of the complexes with the fully aromatic ligands **[(*S/R*)-1]** and **[(*S,S,S/R,R,R*)-2]** appear more intense. However, the most intense ECD signals for **[(*S/R*)-3]** and **[(*S,S,S/R,R,R*)-4]** are expected at a higher energy which are out from the experimental energy range. Similarly to what was observed for $[Dy(hfac)_3((S)/(R)\text{-}L^1)]$ and $[Dy(hfac)_3((S,S,S)/(R,R,R)\text{-}L^3)]$,[52,53] the ECD signals centred at 30000 cm^{-1} (333 nm) and 34000 cm^{-1} (294 nm) for $(S)/(R)\text{-}L^1$ and $(S,S,S)/(R,R,R)\text{-}L^3$ are exalted after the coordination of the achiral $Eu(hfac)_3$ unit in **[(*S/R*)-1]** and **[(*S/R*)-3]**. The same is not observed for **[(*S,S,S/R,R,R*)-2]** and **[(*S,S,S/R,R,R*)-4]**. This might be justified by admitting that the ligands with one stereogenic element undergo a larger structural change after coordination to the $Eu(hfac)_3$ units in solution. The largest absolute values of the dissymmetry factor $|g_{abs}|$ display magnitude order of 10^{-3} (Equation 1, Table 1):

$$g_{abs} = \Delta\varepsilon/\varepsilon = (\varepsilon_L - \varepsilon_R)/(1/2(\varepsilon_L + \varepsilon_R)) \qquad \text{eq. 1}$$

where $\Delta\varepsilon = \varepsilon_L - \varepsilon_R$ is the difference between the left (ε_L) and right (ε_R) molar absorption coefficients at the absorption wavelength.

Table 1 Largest average absolute values of the dissymmetry factor $|g_{abs}|$ in CH_2Cl_2 solution for the two enantiomers of the ligand and related complexes **[(*S/R*)-1]**, **[(*S,S,S/R,R,R*)-2]**, **[(*S/R*)-3]** and **[(*S,S,S/R,R,R*)-4]**.

Ligands and Complexes	Largest $\|g_{abs}\|$ factor	Selected wavelength (nm)
(*S*)/(*R*)-L^1	/*	333
(*S,S,S*)/(*R,R,R*)-L^2	3.80×10^{-3}	260
(*S*)/(*R*)-L^3	/*	333
(*S,S,S*)/(*R,R,R*)-L^4	1.10×10^{-3}	244
[(*S/R*)-1]	1.41×10^{-3}	333
[(*S,S,S/R,R,R*)-2]	3.50×10^{-3}	260
[(*S/R*)-3]	1.14×10^{-3}	333
[(*S,S,S/R,R,R*)-4]	1.24×10^{-3}	244

* Too weak to be measurable at 333 nm

These observations reveal that the metal change induces minimal structural variations.[55] Thus, all complexes present similar largest $|g_{abs}|$ values. The complexes **[(*S/R*)-1]** (1.41×10^{-3}) and **[(*S/R*)-3]** (1.14×10^{-3}) display a strong increase for the $|g_{abs}|$ values compared to the ligands at 30030 cm^{-1} (333 nm), coherently with the increase observed for the ECD signals (Table 1). Conversely, the complexes **[(*S,S,S/R,R,R*)-2]** (3.5×10^{-3}) and **[(*S,S,S/R,R,R*)-4]** (1.24×10^{-3}) exhibit the same order of magnitude for $|g_{abs}|$ than the ligands (*S,S,S*)/(*R,R,R*)-L^2 and (*S,S,S*)/(*R,R,R*)-L^4 respectively at 38461 cm^{-1} (260 nm) and 40984 cm^{-1} (244 nm) (Table 1). These observations could support that the ligands with one stereogenic element undergo a larger structural change than the ligands with three stereogenic element after coordination to the $Eu(hfac)_3$ units in solution.

3.2.2 Luminescence and CPL measurements

For all complexes, red light emission can be visually detected upon excitation at 280 nm (35714 cm^{-1}) in CH_2Cl_2 solution and room temperature. The population of the emissive metal state is reasonably achieved by antenna effect sensitisation.[56] The characteristic bands associated with the $^5D_0 \rightarrow {}^7F_J$ (J = 0-4) transitions for an Eu(III) ion are observed (Figures 1a-4a) with the most intense hypersensitive J=2 band.[57] The minor differences observed between the spectra (*e.g.* splitting, shape, relative peak intensities) can be ascribed to the structural variations provoked by the enantiopure ligands.[57]

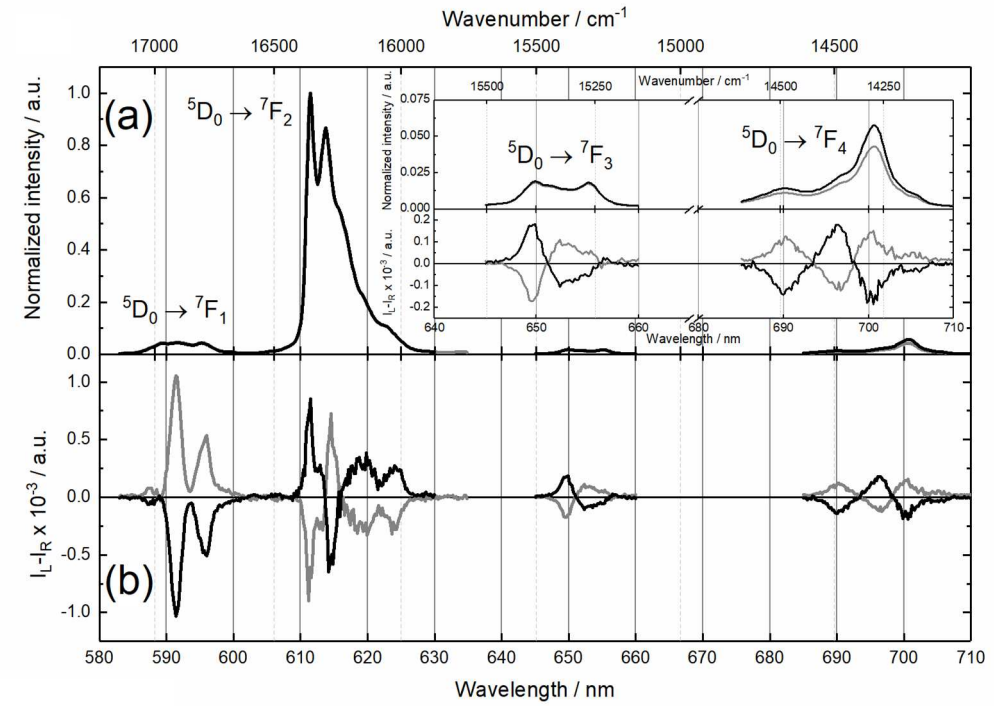

Figure 1. (a) Total emission and (b) CPL spectra measured in CH_2Cl_2 solution under 280 nm (35714 cm^{-1}) irradiation at room temperature for **[(*S*)-1]** (gray line) and **[(*R*)-1]** (black line). Inset: magnification of the range 640–710 nm (15625–14085 cm^{-1}).

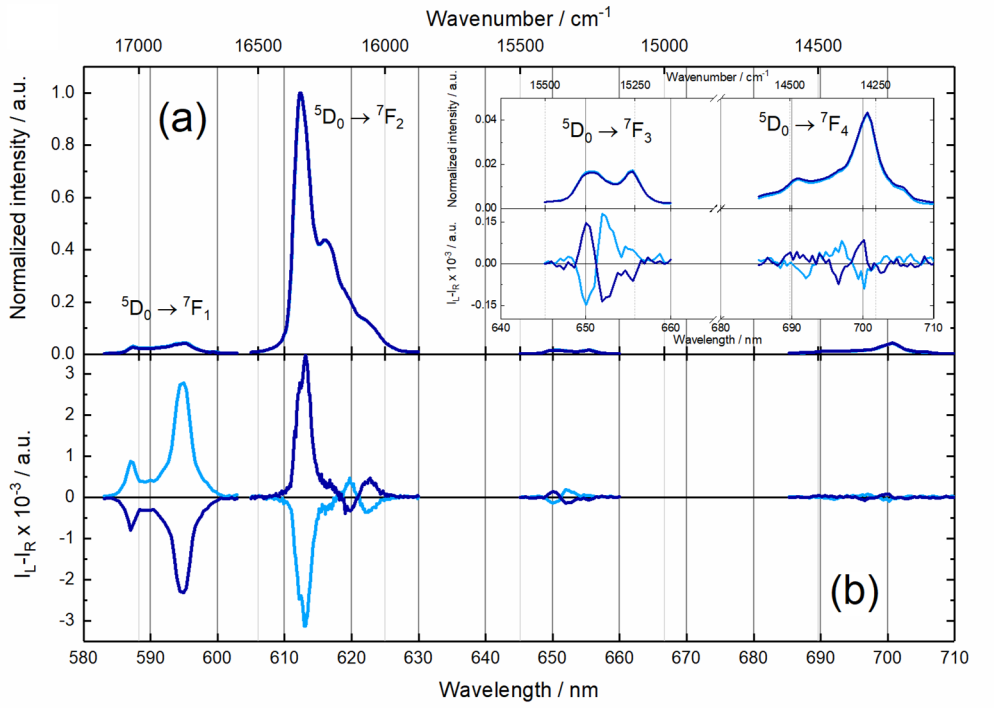

Figure 2. (a) Total emission and (b) CPL spectra measured in CH_2Cl_2 solution under 280 nm (35714 cm^{-1}) irradiation at room temperature for **[(*S*,*S*,*S*)-2]** (light blue line) and **[(*R*,*R*,*R*)-2]** (dark blue line). Inset: magnification of the range 640–710 nm (15625–14085 cm^{-1}).

The Gaussian shape for the single $^5D_0 \rightarrow {}^7F_0$ transition of **[(*S/R*)-1]** (Figure S20a) indicated the presence of a single species in dichloromethane solution assigned to a monomeric structure according to the combined NMR and DFT studies previously published.[52] By analogy, the single $^5D_0 \rightarrow {}^7F_0$ transition observed for the others compounds **[(*S,S,S/R,R,R*)-2]**, **[(*S,R*)-3]** and **[(*S,S,S/R,R,R*)-4]** (Figure S20b-d), suggests the formation of the monomeric compounds in solution for the complete series. The $^5D_0 \rightarrow {}^7F_2$ transitions depict a significant hypersensitivity, which is commonly reported for europium β-diketonato complexes (Figure S20a-d).[58] The shape of the $^5D_0 \rightarrow {}^7F_2$ transition is similar for the species **[(*S/R*)-1]** and **[(*S,R*)-3]**, or **[(*S,S,S/R,R,R*)-2]** and **[(*S,S,S/R,R,R*)-4]**. Nevertheless the ratio R of the intensities of the transition $^5D_0 \rightarrow {}^7F_2$ and $^5D_0 \rightarrow {}^7F_1$ ($R = I(^5D_0 \rightarrow {}^7F_2)/I(^5D_0 \rightarrow {}^7F_1)$) is found close for all the compounds i.e. 23.0 for **[(*S/R*)-1]**, 21.8 for **[(*S,S,S/R,R,R*)-2]**, 20.6 for **[(*S,R*)-3]** and 20.2 for **[(*S,S,S/R,R,R*)-4]**, highlighting a similar symmetry of the Eu(III) site in the compound series. It is worth noticing that a value of R > 10 is commonly observed for Eu(III) β-diketonate complexes.[59-64] The emission decay curves can be fitted by mono-exponential functions (Figure S21) confirming the presence of single spectroscopic Eu(III) site and thus supporting the existence of single monomeric species in solution. The order of magnitude of the observed lifetimes (τ_{obs}) is the same for all the samples (Tables 2 and 3). The τ_{obs} magnitude is coherent with the values observed for some literature tris(β-diketonate) complexes with ligands bearing P=O donor groups.[39]

Table 2. Experimental lifetime (τ_{obs}) for the europium compounds in CH_2Cl_2 solution excited at 330 nm (30303 cm^{-1}).

Compounds	τ_{obs} (ms)	
	(*S*) enantiomer	(*R*) enantiomer
[(*S/R*)-1]	0.61	0.66
[(*S,S,S/R,R,R*)-2]	0.48	0.46
[(*S/R*)-3]	0.66	0.64
[(*S,S,S/R,R,R*)-4]	0.47	0.48

The differential emission between left and right circularly polarized light for all the Eu(III) complexes was measured in solution at room temperature.

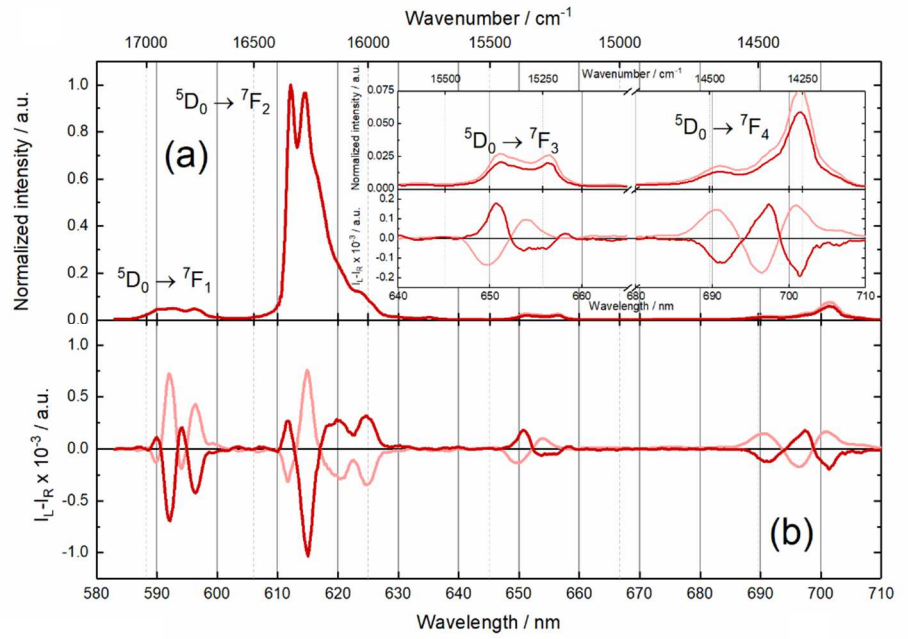

Figure 3. (a) Total emission and (b) CPL spectra measured in CH_2Cl_2 solution under 280 nm (35714 cm^{-1}) irradiation at room temperature for **[(*S*)-3]** (light red line) and **[(*R*)-3]** (dark red line). Inset: magnification of the range 640–710 nm (15625–14085 cm^{-1}).

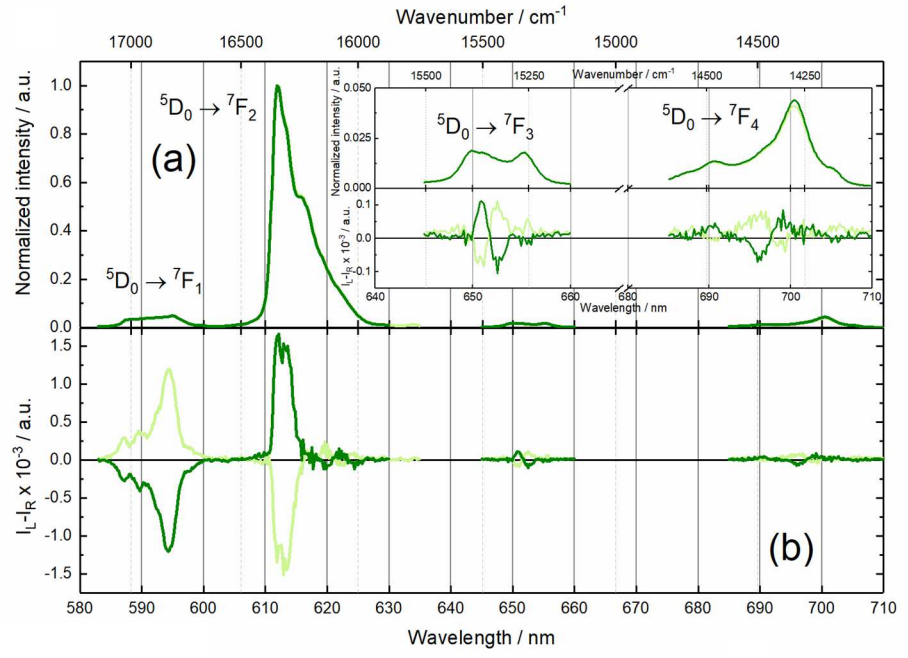

Figure 4. (a) Total emission and (b) CPL spectra measured in CH_2Cl_2 solution under 280 nm (35714 cm^{-1}) irradiation at room temperature for **[(*S,S,S*)-4]** (light green line) and **[(*R,R,R*)-4]** (dark green line). Inset: magnification of the range 640–710 nm (15625–14085 cm^{-1}).

Symmetrical CPL signals are recorded for each enantiomeric pair (Figures 1-4b). Thus, the following discussion is given for the (*S*) enantiomers. Except for the $^5D_0 \rightarrow {}^7F_0$ transition that is not visible in CPL, a correspondence between the CPL and luminescence transitions can be clearly detected (Figures 1-4). Similarities between the compounds are observed in the CPL studies as well. For instance, the main signals of the $^5D_0 \rightarrow {}^7F_1$ transition is positive (+) for the complexes **[(*S*)-1]** and **[(*S*)-3]**. It is worth to notice that more than 3 contributions could be observed for the $^5D_0 \rightarrow {}^7F_1$ transition. Such fact might be due to the flexibility of the coordination system in solution and/or to vibronic contribution. At the same transitions, the first contribution is more intense than the second. At the $^5D_0 \rightarrow {}^7F_2$ transition, four signals with signs negative/positive/negative/negative (–/+/–/–) are identified. A certain correspondence in shape and sign is also observed for the $^5D_0 \rightarrow {}^7F_3$ and $^5D_0 \rightarrow {}^7F_4$ transitions. The CPL spectra of the compounds **[(*S,S,S*)-2]** and **[(*S,S,S*)-4]** are similar in shape and sign. For instance, the signs of the main $^5D_0 \rightarrow {}^7F_1$ and $^5D_0 \rightarrow {}^7F_2$ transitions are (+) and (–), respectively. The sign relation is conserved also for the $^5D_0 \rightarrow {}^7F_3$ and $^5D_0 \rightarrow {}^7F_4$ transitions. Furthermore, the first contributions of the $^5D_0 \rightarrow {}^7F_1$ transitions are less intense than the last, differently than for **[(*S*)-1]** and **[(*S*)-3]**. By comparing all the complexes, the largest CPL signals at the $^5D_0 \rightarrow {}^7F_1$ are (+). At the $^5D_0 \rightarrow {}^7F_3$ transition all the compounds display similar features. Conversely, the sign and intensity at the $^5D_0 \rightarrow {}^7F_4$ transition seem dependent on the nature of the chiral ligand (*e.g.* (+/–/+/+) for **[(*S*)-1]** and **[(*S*)-3]** and (–/+/–) for **[(*S,S,S*)-2]** and **[(*S,S,S*)-4]**. In other words, the general feature of the CPL spectra might be associated with the number of stereogenic elements, one for **[(*S*)-1]** and **[(*S*)-3]** and three for **[(*S,S,S*)-2]** and **[(*S,S,S*)-4]**. In other words, the feature of the CPL spectra might depend of the steric hindrance of the ligand which leads to variation of the coordination sphere around the Eu(III) centre.

The g_{lum} values are reported in Tables S4-S7. As commonly observed,[65] the $|g_{lum}|$ values at the magnetic-dipole transition $^5D_0 \rightarrow {}^7F_1$ are the largest. At this transition, the average $|g_{lum}|$ values between the two enantiomers for **[(*S/R*)-1]** ($|{}^{max}g_{lum}| = 4.7\times10^{-2}$ at 591 nm), **[(*S/R*)-3]** ($|{}^{max}g_{lum}| = 2.8\times10^{-2}$ at 592 nm) and **[(*S,S,S/R,R,R*)-4]** ($|{}^{max}g_{lum}| = 5.3\times10^{-2}$ at 594 nm) display comparable values which approach the literature data for similar systems.[39,40] Conversely, the g_{lum} values for **[(*S,S,S/R,R,R*)-2]** ($|{}^{max}g_{lum}| = 0.12$ at 595 nm) are remarkably increased. At the $^5D_0 \rightarrow {}^7F_1$ transition the following trend could be proposed looking at the larger g_{lum} values ($^{max}g_{lum}$) of each compound $|{}^{max}g_{lum}|$**[(*S,S,S/R,R,R*)-2]** > $|{}^{max}g_{lum}|$**[(*S,S,S/R,R,R*)-4]** > $|{}^{max}g_{lum}|$**[(*S/R*)-1]** > $|{}^{max}g_{lum}|$**[(*S/R*)-3]** (Table 3). Analyzing the proposed $|{}^{max}g_{lum}|$ values trend, one might propose that the ligand with π-extended system/more rigid system and

three stereogenic elements might benefit the $|g_{lum}|$ magnitude at the magnetic transition. The $|g_{lum}|$ values at the other transitions do not seem affected by the change of the ligand (Tables S4-S7).

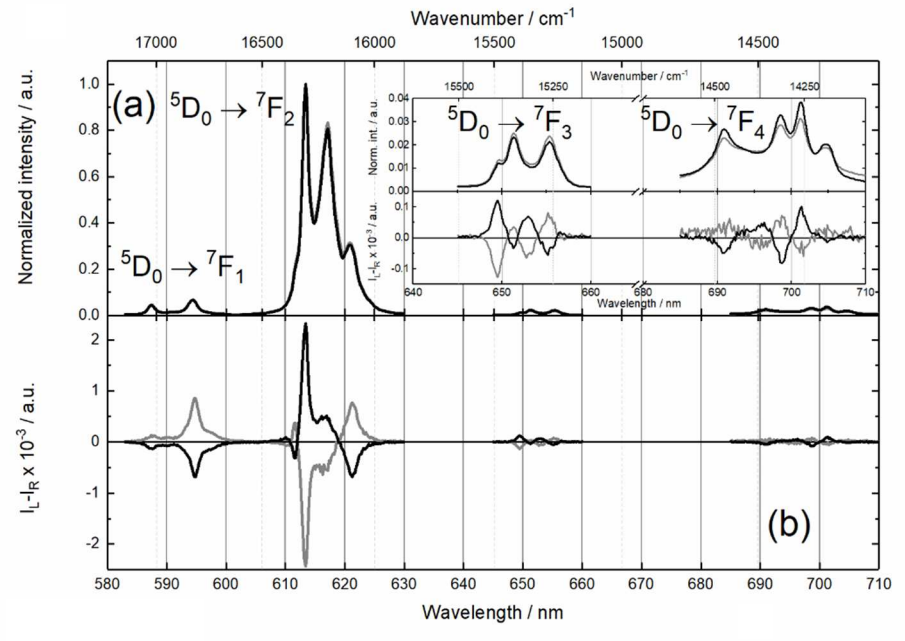

Figure 5. (a) Total emission and (b) CPL spectra measured in solid-state under 340 nm (29412 cm^{-1}) irradiation at room temperature for **[(*S*)-1]$_n$** (gray line) and **[(*R*)-1]$_n$** (black line). Inset: magnification of the range 640–710 nm (15625–14085 cm^{-1}).

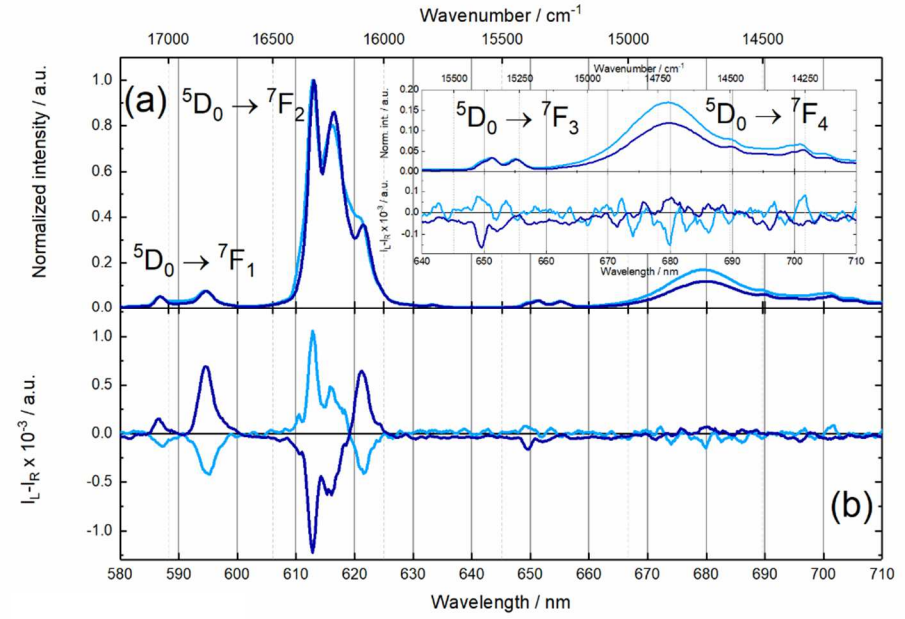

Figure 6. (a) Total emission and (b) CPL spectra measured in solid-state under 340 nm (29412 cm^{-1}) irradiation at room temperature for **[(*S*,*S*,*S*)-2]$_n$** (light blue line) and **[(*R*,*R*,*R*)-2]$_n$** (dark blue line). Inset: magnification of the range 640–710 nm (15625–14085 cm^{-1}).

The luminescence properties of the four polymeric compounds were also studied in the solid state. Irradiation at 340 nm (29412 cm^{-1}) of **[(*S/R*)-1]$_n$**, **[(*S,S,S/R,R,R*)-2]$_n$**, **[(*S,R*)-3]$_n$** and **[(*S,S,S/R,R,R*)-4]$_n$** led to the observation of the characteristic Eu(III) centered emission (Figures 5a-8a).

The emission single-decay curves (Figure S22) allow to determine τ_{obs} values of the same order of magnitude than in solution (Table S8). Comparable solid state τ_{obs} values are reported for some similar literature species.[66,67]

The CPL emission is also studied in solid state for the four polymers **[(*S/R*)-1]$_n$**, **[(*S,S,S/R,R,R*)-2]$_n$**, **[(*S,R*)-3]$_n$** and **[(*S,S,S/R,R,R*)-4]$_n$** (Figures 5b-8b). In most of the transitions the CPL signs of **[(*S/R*)-1]$_n$** and **[(*S,R*)-3]$_n$** or **[(*S,S,S/R,R,R*)-2]$_n$** and **[(*S,S,S/R,R,R*)-4]$_n$** are the same while they appear inverted for a given enantiomer when comparing the polymers involving the binaphtyl ligands with one stereogenic elements and those involving three stereogenic elements. The CPL spectra for the three compounds **[(*S/R*)-1]$_n$**, **[(*S,R*)-3]$_n$** and **[(*S,S,S/R,R,R*)-4]$_n$** display a relatively similar profile. The g_{lum} values are reported in Tables S9-S12 and the $|g_{lum}|$ magnitudes for the four compounds are comparable. Indeed, $|^{max}g_{lum}|$ values, which correspond to the magnetic-dipole transitions, are 0.024 (at 594.7 nm), 0.028 (at 595.4 nm), 0.016 (at 592.6 nm) and 0.024 (at 590.8 nm) for **[(*S/R*)-1]$_n$** and **[(*S,R*)-3]$_n$** or **[(*S,S,S/R,R,R*)-2]$_n$** and **[(*S,S,S/R,R,R*)-4]$_n$**, respectively (Table 3).

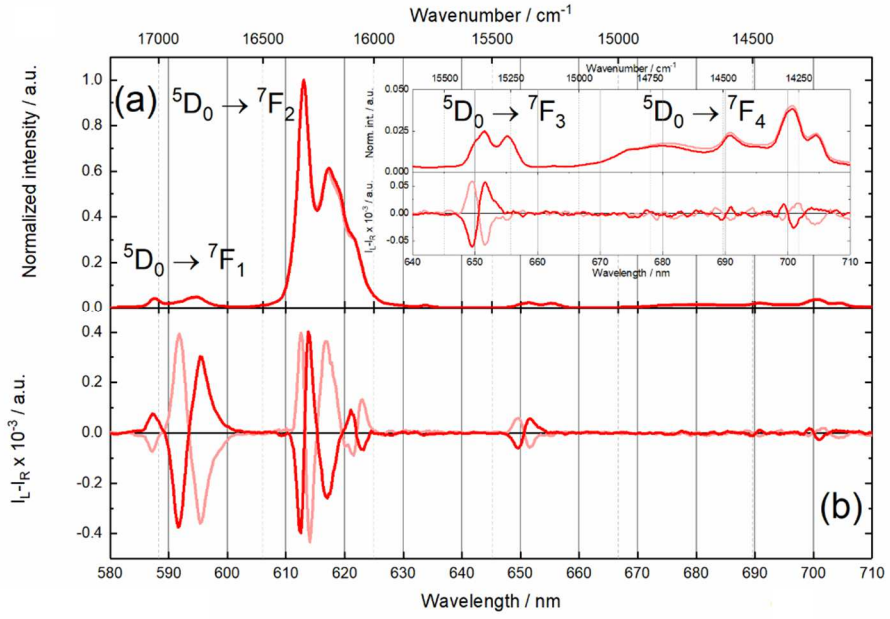

Figure 7. (a) Total emission and (b) CPL spectra measured in solid-state under 340 nm (29412 cm^{-1}) irradiation at room temperature for **[(*S*)-3]$_n$** (light red line) and **[(*R*)-3]$_n$** (dark red line). Inset: magnification of the range 640–710 nm (15625–14085 cm^{-1}).

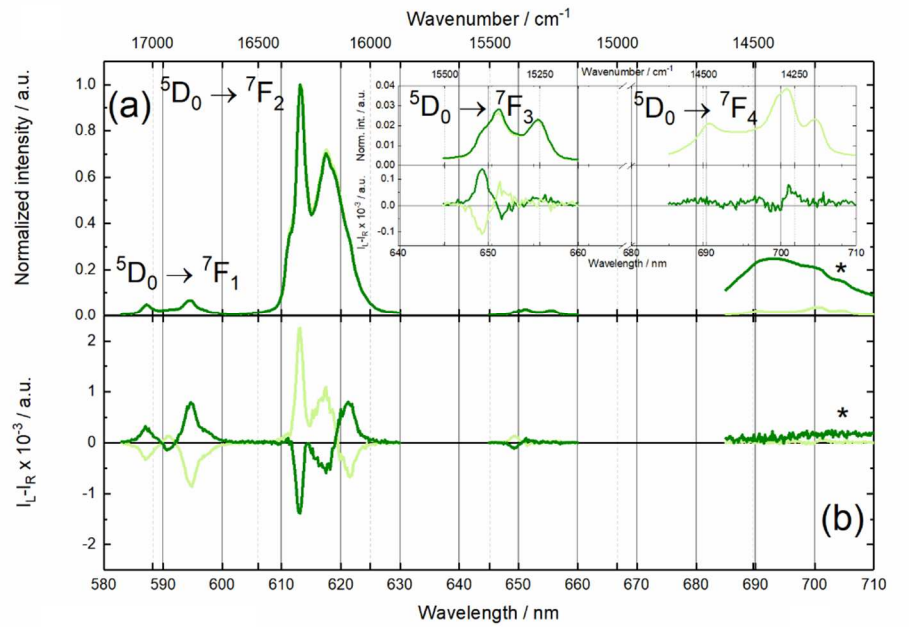

Figure 8. (a) Total emission and (b) CPL spectra measured in solid-state under 340 nm (29412 cm^{-1}) irradiation at room temperature for **[(*S,S,S*)-4]$_n$** (light green line) and **[(*R,R,R*)-4]$_n$** (dark green line). Inset: magnification of the range 640–710 nm (15625–14085 cm^{-1}).

Table 3. Selected parameters of the (chir)optical properties for the four Eu(III) compounds.

	Solution (n=1)			Solid-state	
	g_{abs}	Lifetime	$^{max}g_{lum}$	Lifetime	$^{max}g_{lum}$
[(*S/R*)-1]$_n$	1.41×10^{-3}	0.64 ms	4.7×10^{-2}	0.78 ms	2.4×10^{-2}
[(*S,S,S/R,R,R*)-2]$_n$	3.50×10^{-3}	0.47 ms	0.12	0.55 ms	1.6×10^{-2}
[(*S,R*)-3]$_n$	1.14×10^{-3}	0.65 ms	2.8×10^{-2}	0.80 ms	2.8×10^{-2}
[(*S,S,S/R,R,R*)-4]$_n$	1.24×10^{-3}	0.48 ms	5.3×10^{-2}	0.66 ms	2.4×10^{-2}

* The given values are average values for the two enantiomers.

The electric-dipole transitions show $|g_{lum}|$ values of 4.8×10^{-3} (at 613.4 nm), 8.9×10^{-4} (at 612.5 nm), 2.0×10^{-3} (at 612.8 nm) and 3.9×10^{-3} (at 612.9 nm) for **[(*S/R*)-1]$_n$** and **[(*S,R*)-3]$_n$** or **[(*S,S,S/R,R,R*)-2]$_n$** and **[(*S,S,S/R,R,R*)-4]$_n$**, respectively.

One could remark that the two compounds involving the ligands with three stereogenic elements inverted their CPL contribution signs from solution to solid-state. Inversion of CPL sign was already observed in the literature depending of the solvent nature,[68] aggregation[69] and matrix nature.[70] Nevertheless the conversion of the polymeric nature of the compounds in solid-

state into monomeric one in CH_2Cl_2 solution which is accompanied with a drastic reorganization of the Eu(III) coordination sphere as well as the coordination mode of the chiral ligand lead to absence of obvious relation between CPL measurements in solution and solid-state.

4. CONCLUSION

In conclusion, four polymeric compounds of formula $\{[Ln(hfac)_3((S)/(R)\text{-}L^x)]\}_n$ (x = 1-4) have been synthetized and characterized by PXRD. Their CPL spectra have been recorded in both CH_2Cl_2 solution and solid-state. The shape of the CPL spectra in solution can be classified depending of the number of stereogenic centers of the chiral ligand. The extraction of the g_{lum} factor highlighted that the highest values correspond to the magnetic-dipole transitions as expected and the highest $|g_{lum}|$ value has been found for the complex involving the chiral ligand with the most extended π system and three stereogenic elements. To the best of our knowledge, the **[(*S,S,S/R,R,R*)-2]** complex displays the highest $g_{lum} = 0.12$ observed for an $Eu(hfac)_3$-based compound involving a binaphtyl-based ligand.

Solid-state CPL measurements revealed inversion of sign for most of the contributions for **[(*S,S,S/R,R,R*)-2]$_n$** and **[(*S,S,S/R,R,R*)-4]$_n$** compared to **[(*S/R*)-1]$_n$** and **[(*S,R*)-3]$_n$** as well as significant difference with CPL spectra in solution that can be explained by the conversion of the polymeric structures in solid-state into monomers in solution.

ACKNOWLEDGEMENTS

This work was supported by CNRS, Université de Rennes and the European Research Council through the ERC-CoG 725184 MULTIPROSMM (project no. 725184) and the Agence Nationale de la Recherche (SMMCPL ANR-19-CE29-0012-02). Part of this work has been performed using the Spectroscopies-DCTP core facility (UMS Biosit, Université de Rennes 1-Campus de Villejean - 35043 RENNES Cedex, FRANCE).

REFERENCES

1. Riehl JP, Richardson FS. Circularly polarized luminescence spectroscopy. *Chem Rev.* 1986;86(1):1-16.
2. Carr, R, Evans, NH, Parker, D. Lanthanide complexes as chiral probes exploiting circularly polarized luminescence. *Chem Soc Rev.* 2012;41:7673–7686.

3. Urey H, Chellappan KV, Erden E, Surman P. State of the art in stereoscopic and autostereoscopic displays. *Proc IEEE*. 2011;99(4):540-555.
4. Bennett CH, DiVincenzo DP. Quantum information and computation. *Nature*. 2000;404(6775):247 - 255.
5. Jennings L, Waters RS, Pal R, Parker D. Induced europium circularly polarized luminescence monitors reversible drug binding to native A1-acid glycoprotein. *ChemMedChem*. 2017;12(3):271-277.
6. Neil ER, Fox MA, Pal R, Parker D. Induced europium CPL for the selective signaling of phosphorylated amino-acids and O-phosphorylated hexapeptides. *Dalton Trans*. 2016;45(20): 8355 - 8366.
7. Ray C, Sánchez - Carnerero EM, Moreno F, et al. Bis(HaloBODIPYs) with labile helicity: valuable simple organic molecules that enable circularly polarized luminescence. *Chem Eur J.* 2016;22(26):8805-8808.
8. Sánchez-Carnerero EM, Agarrabeitia AR, Moreno F, et al. Circularly polarized luminescence from simple organic molecules. *Chem Eur J.* 2015;21(39):13488-13500.
9. Saleh N, Moore B, Srebro M, et al. Acid/base-triggered switching of circularly polarized luminescence and electronic circular dichroism in organic and organometallic helicenes. *Chem Eur J.* 2015;21(4):1673-1681.
10. Alnoman RB, Rihn S, O'Connor DC, et al. Circularly polarized luminescence from helically chiral N,N,O,O-boron-chelated dipyrromethenes. *Chem Eur J.* 2016;22(1):93 - 96.
11. Feuillastre S, Pauton M, Gao L, et al. Design and synthesis of new circularly polarized thermally activated delayed fluorescence emitters. *J Am Chem Soc.* 2016;138(12):3990-3993.
12. Kono Y, Nakabayashi K, Kitamura S, Kuroda R, Fujiki M, Imai Y. A comparison of circularly polarised luminescent BINAP and BINAPO as chiral binaphthyl luminophores. *Tetrahedron.* 2015;71(23):3985-3989.
13. Delgado IH, Pascal S, Wallabregue A, et al. Functionalized cationic [4] helicenes with unique tuning of absorption, fluorescence and chiroptical properties up to the far-red range. *Chem Sci.* 2016;7(7):4685 - 4693.
14. Sannicolò F, Mussini PR, Benincori T, et al. Inherently chiral macrocyclic oligothiophenes: easily accessible electrosensitive cavities with outstanding enantioselection performances. *Chem Eur J.* 2014;20(47):15298-15302.

15. Pascal S, Besnard C, Zinna F, et al. Zwitterionic [4] helicene: a water-soluble and reversible PH-triggered ECD/CPL chiroptical switch in the UV and red spectral regions. *Org Biomol Chem.* 2016;14(20):4590-4594.
16. Zhao B, Pan K, Deng J. Intense circularly polarized luminescence contributed by helical chirality of monosubstituted polyacetylenes. *Macromolecules.* 2018;51(18):7104-7111.
17. Dhbaibi K, Favereau L, Crassous J. Enantioenriched Helicenes and Helicenoids Containing Main-Group Elements (B, Si, N, P), *Chem Rev.* 2019;119:8846–8953.
18. Leonzio M, Bettinelli M, Arrico L, Monari M, Di Bari L, Piccinelli F. Circularly Polarized Luminescence from an Eu(III) Complex Based on 2-Thenoyltrifluoroacetyl-acetonate and a Tetradentate Chiral Ligand. *Inorg Chem.* 2018;57(16):10257–10264.
19. Zinna F, Arrico L, Di Bari L. Near-infrared circularly polarized luminescence from chiral Yb(III)-diketonates. *Chem Commun.* 2019;55:6607–6609.
20. Burrezo PM, Jiménez VG, Blasi D, Ratera I, Campana AG, Veciana J. Organic Free Radicals as Circularly Polarized Luminescence Emitters. *Angew Chem Int Ed.* 2019;58:16282–16288.
21. Isla H, Saleh N, Ou-Yang JK, et al. Bis-4-aza[6]helicene : A Bis-helicenic 2,2'-Bipyridine with Chemically Triggered Chiroptical Switching Activity. *J. Org. Chem.* 2019;84(9):5383–5393.
22. Guy L, Mosser M, Pitrat D, et al. Modulation of Chiroptical Properties in a Series of helicene-like Compounds. *J Org Chem.* 2019;84(17):10870–10876.
23. Zinna F, Di Bari L. Lanthanide circularly polarized luminescence: bases and applications. *Chirality*. 2015;27(1):1-13
24. Richardson FS, Faulkner TR. Optical activity of the f–f transitions in trigonal dihedral (D3) lanthanide (III) complexes. I. Theory. *J Chem Phys.* 1982;76(4):1595-1606.
25. Lunkley JL, Shirotani D, Yamanari K, Kaizaki S, Muller G. Extraordinary Circularly Polarized Luminescence Activity Exhibited by Cesium Tetrakis(3-heptafluoro-butylryl-(+)-camphorato) Eu(III) Complexes in EtOH and $CHCl_3$ Solutions. *J Am Chem Soc.* 2008;130(42):13814–13815.
26. Leonzio M, Melchior A, Faura G, et al. Strongly circularly polarized emission from water-soluble Eu (III)- and Tb (III)- based complexes: a structural and spectroscopic study. *Inorg Chem.* 2017;56(8):4413-4421.
27. Kono Y, Hara N, Shizuma M, Fujiki M, Imai Y. Complexes of Eu(III)$(Hfa)_3$ with a planar chiral P(III) ligand (phanephos): solvent-sensitive sign inversion of circularly polarised luminescence. *Dalton Trans.* 2017;46(16):5170-5174.

28. Casanovas B, Zinna F, Bari LD, Fallah MSE, Font-Bardía M, Vicente R. Circularly polarized luminescence on dinuclear Tb(III) and Eu(III) complexes with (S-) and (R-) 2- phenylpropionate. *Dalton Trans.* 2017;46(19):6349 - 6357.
29. Zercher B, Hopkins TA. Induction of circularly polarized luminescence from europium by amino acid based ionic liquids. *Inorg Chem.* 2016;55(21):10899-10906.
30. Dai L, Lo W-S, Coates ID, Pal R, Law G-L. New class of bright and highly stable chiral cyclen europium complexes for circularly polarized luminescence applications. *Inorg Chem.* 2016;55(17):9065-9070.
31. Uchida T, Nozaki K, Iwamura M. Chiral sensing of various amino acids using induced circularly polarized luminescence from europium(III) complexes of phenanthroline dicarboxylic acid derivatives. *Chem – Asian J.* 2016;11(17):2415-2422.
32. Kitagawa Y, Tsurui M, Hasegawa Y. Steric and Electronic Control of Chiral Eu(III) Complexes for Effective Circularly Polarized Luminescence. *ACS Omega.* 2020;5(8):3786-3791.
33. Arrico L, De Rosa C, Di Bari L, Melchior A, Piccinelli F. Effect of the Counterion on Circularly Polarized Luminescence of Europium(III) and Samarium(III) Complexes. *Inorg Chem.* 2020;59(7):5050-5062.
34. Cui M, Wang AL, Gao CL, et al. Two homochiral Eu^{III} and Sm^{III} enantiomeric pairs showing circularly polarized luminescence, photoluminescence and triboluminescence. *Dalton Trans.* 2021;50:1007-1018.
35. Bünzli J-CG. Lanthanide luminescence for biomedical analyses and imaging. *Chem Rev.* 2010;110(5):2729-2755.
36. D'Aléo A, Pointillart F, Ouahab L, Andraud C, Maury O. Charge transfer excited states sensitization of lanthanide emitting from the visible to the near-infra-red. *Coord Chem Rev.* 2012;256:1604-1620.
37. Gendron F, Di Pietro S, Abad Galan L, et al. Luminescence, chiroptical, magnetic and ab initio crystal-field characterizations of an enantiopure helicoidal Yb(III) complex. *Inorg Chem Front.* 2021;8:914-926.
38. Lefeuvre B, Mattei CA, Flores Gonzalez J, et al. Solid-State Near-Infrared Circularly Polarized Luminescence from Chiral Yb^{III}-Single-Molecule Magnet. *Chem Eur J.* 2021;27:7362-7366.
39. Harada T, Nakano Y, Fujiki M, Naita M, Kawai T, Hasegawa Y. Circularly Polarized Luminescence of Eu(III) Complexes with Point- and Axis-Chiral Ligands Dependent on Coordination Structures. *Inorg Chem.* 2009;48(23):11242-11250.

40. Koiso N, Kitagawa Y, Nakanishi T, Fushimi K, Hasegawa Y. Eu(III) Chiral Coordination Polymer with a Structural Transformation System. *Inorg Chem.* 2017;56(10):5741–5747.
41. Liu D, Zhou Y, Zhang Y, et al. Chiral BINAPO-Controlled Diastereoselective Self-Assembly and Circularly Luminescence in Triple-Stranded Europium(III) Podates. *Inorg Chem.* 2018;57(14):8332–8337;
42. A. J. Jalilah, F. Asanoma, M. Fujiki, *Inorg. Chem. Front.* 2018, *5*, 2718–2733.
43. Zhou Y, Li H, Zhu T, Gao T, Yan P. A Highly Luminescent Chiral Tetrahedral $Eu_4L_4(L')_4$ Cage : Chirality Induction, Chirality Memory, and Circularly Polarized Luminescence. *J Am Chem Soc.* 2019;141(50):19634-19643.
44. Tsurui M, Kitagawa Y, Fushimi K, Gon M, Tanaka K, Hasegawa Y. Electronic strain effect on Eu(III) complexes for enhanced circularly polarized luminescence. *Dalton Trans.* 2020;49:5353-5361.
45. Deng M, Schley ND, Ung G. High circularly polarized luminescence brightness from analogues of Shibasaki's lanthanide complexes. *Chem. Commun.* 2020;56:14813-14816.
46. Dai L, Lo WS, Coates ID, Pal R, Law GL. New Class of bright and Highly Stable Chiral Cyclen Europium Complexes for Circularly Polarized Luminescence Applications. *Inorg Chem.* 2016, 55(17):9065-9070.
47. Homberg A, Brun E, Zinna F. Combined reversible switching of ECD and quenching of CPL with chiral fluorescent macrocycles. *Chem Sci.* 2018;9:7043-7052.
48. Ngo Ndimba A, Roisnel T, Argouarch G, Lalli C. Harvesting New Chiral Phosphotriesters by Phosphorylation of BINOL and Parent Bis-phenols, *Synthesis.* 2019;51:865–873.
49. Richardson MF, Wagner WF, Sands, DE. Rare earth trishexafluoroacetylacetonates and related compounds. *J Inorg Nucl Chem.* 1968;30:1275–1289.
50. Sheldrick GM, SHELXT – Integrated space-group and crystal-structure determination, *Acta Crystallogr, Sect A: Found Adv.* 2015;71:3–8.
51. Sheldrick GM, Crystal structure refinement with SHELXL, *Acta Crystallogr, Sect C: Struct Chem.* 2015;71:3–8.
52. Mattei CA, Montigaud V, gendron F, et al. Solid-state versus solution investigation of a luminescent chiral BINOL-derived bisphosphate single-molecule magnet. *Inorg Chem Front.* 2021;8:947-962.

53. Mattei CA, Montigaud V, Dorcet V, et al. Luminescent dysprosium single-molecule magnets made from designed chiral BINOL-derived bisphosphate ligands. *Inorg Chem Front.* 2021;8:963-976.
54. Pointillart F, Jung J, Berraud-Pache R, et al. Luminescence and Single-Molecule Magnet Behavior in Lanthanide Complexes Involving a Tetrathiafulvalene-Fused Dipyridophenazine Ligand, *Inorg Chem.* 2015;54(11):5384–5397.
55. Górecki M, Carpita L, Arrico L, Zinna F, Di Bari L. Chiroptical Methods in a Wide Wavelength Range for Obtaining Ln3+ Complexes with Circularly Polarized Luminescence of Practical Interest. *Dalton Trans.* 2018;47(21):7166–7177.
56. *Molecular Magnetic Materials: Concepts and Applications*; Sieklucka, B., Pinkowicz, D., Eds.; Wiley-VCH Verlag GmbH & Co. KGaA, 2017.
57. Binnemans, K. Interpretation of Europium(III) Spectra. *Coord. Chem. Rev.* 2015;295:1–45.
58. Bellucci L, Bottaro G, Labella L, et al. Composition–Thermometric Properties Correlations in Homodinuclear Eu 3+ Luminescent Complexes. *Inorg. Chem.* 2020;59(24):18156–18167.
59. Lunstroot K, Driesen K, Nockemann P, et al. Luminescent ionogels Based on Europium-Doped Ionic Liquids Confined within Silica-Derived Networks. *Chem. Mater.* 2006;18:5711–5715.
60. Lunstroot K, Driesen K, Nockemann P, et al. Lanthanide-doped luminescent ionogels. *Dalton Trans.* 2009:298–306.
61. Binnemans K, Moors D. Narrow band photoluminescence of europium-doped liquid crystals. *J Mater Chem.* 2002;12:3374–3376.
62. Brito HF, Malta OL, Menezes JFS, Luminescent properties of diketonates of trivalent europium with dimethyl sulfoxide. *J Alloys Compd.* 2000;303:336–339.
63. Bünzli JCG, Moret E, Foiret V, Schenk KJ, Wang MZ, Jin LP. Structural and photophysical properties of europium(III) mixed complexes with β-diketonates and *o*-phenantroline. *J. Alloys Compd.* 1994;207:107–111.
64. Feng M, Pointillart F, Le Guennic B, Lefeuvre B, Golhen S, Cador O, Maury O, Ouahab L. Unprecedended Sensitization of Visible and Near-infrared Lanthanide Luminescence bu using a tetrathiafulvalene-Based Chromophore. *Chem Asian J.* 2014;9:2814-2825.
65. Arrico L, Di Bari L, Zinna F. Quantifying the Overall Efficiency of Circularly Polarized Emitters. *Chem Eur J.* 2020;27(9):2920–2034.

66. Hirai Y, Nakanishi T, Hasegawa Y. Organo-Lanthanide Luminophores Bridged by Phosphine Oxide Ligands. *J Lumin.* 2016;170:801–807.
67. Hasegawa Y, Natori S, Fukudome J, et al. Effective Europium Coordination Luminophores Linked with Bi- and Tridentate Carbazole Phosphine Oxides for Organic Electroluminescent Devices. *J Phys Chem. C* 2018;122(17):9599–9605.
68. Nagata Y, Nishikawa T, Suginome M. Chirality-switchable circularly polarized luminescence in solution based on the solvent-dependent helix inversion of poly(quinoxaline-2,3-diyls)s. *Chem Commun.* 2014; 50:9951-9953.
69. Sheng Y, Ma J, Liu S, Wang Y, Zhu C, Cheng Y. Strong and Reversible Circularly Polarized Luminescence Emission of a Chiral 1,8-Naphthalimide Fluorophore Induced by Excimer Emission and orderly Aggregation. *Chem Eur J.* 2016;22,9519-9522.
70. Kimoto T, Amako T, Tajima N, Kuroda R, Fujiki M, Imai Y. Control of Solid-state Circularly Polarized Luminescence of Binaphthyl Organic Fluorophores through Environmental Changes. *Asian J Org Chem.* 2013;2:404-410.